Hindawi
Material Design & Processing Communications
Volume 2022, Article ID 4566471, 9 pages
https://doi.org/10.1155/2022/4566471

Research Article

Maximum Inclusion Size Evaluation and Fatigue Strength Analysis of 40Cr Structural Steel

Yingxin Zhao[1] **and Aiguo Zhao**[2]

[1]*Standards & Metrology Research Institute, China Academy of Railway Sciences Corporation Limited, Beijing 10081, China*
[2]*College of Civil Engineering, Nanjing Tech University, Nanjing 211816, China*

Correspondence should be addressed to Yingxin Zhao; yxzhao15801042226@163.com

Received 22 February 2022; Revised 22 March 2022; Accepted 31 March 2022; Published 30 April 2022

Academic Editor: Guian Qian

Statistics of extreme values (SEV) and generalized Pareto distribution (GPD) are adopted to predict the maximum inclusion size in 40Cr structural steel, and the fatigue strength was estimated according to the obtained maximum inclusion size. The estimated results were compared with the experimental results obtained in rotating bending fatigue testing, where all failure-relevant inclusions of the present study were quantitatively analyzed with respect to $\sqrt{\text{area}}$ (square root of the projected inclusion area). Both the estimation results are consistent with the experimental results. Furthermore, a suitable maximum inclusion size equal to the prior austenite grain size is proposed for the material manufacturing process.

1. Introduction

The fatigue performance of mechanical components during service is the most important aspect in the design of engineering structures [1–3]. The fatigue lifetimes of materials are influenced by many factors, while inclusions have considerable adverse effects on the mechanical properties of materials [4–10]. In the low cycle fatigue and high cycle fatigue regime, fractures appear on the material surfaces, and in the very high cycle fatigue regime, cracks initiate from internal defects such as inclusions, voids, and microscopic nonuniformities. Related experimental results indicate that internal inclusions become the most likely fracture origin in very high cycle fatigue regime, especially the large inclusions at the adjacent surfaces, which will cause quick fracture initiation [7, 9]. The size and randomness distribution of inclusions will greatly scatter the fatigue life, and there is a variation in fatigue life of 2~3 orders of magnitude at a given loading amplitude [3, 4]. Murakami has conducted a systematical study on the effects of inclusions and proposed the $\sqrt{\text{area}}$ (square root of the projected inclusion area) semiempirical model [6]. The model could be utilized to predict the fatigue strength, and the scatter of fatigue data was substantially reduced through modification of the model. Therefore, the estimation of the maximum inclusion size is of great importance for estimating the fatigue strength of materials. Many methods are employed to inspect the inclusions of metal materials, such as metallographic method, nondestructive testing, inclusion concentration method, and fatigue fracture analysis method [1, 6]. The determination of the maximum inclusion size (or other defects) in a specimen usually represents a difficult challenge due to their low probability of occurrence. However, methods based on the statistics of extreme values enable the estimation of maximum inclusion size as well as the quantitative description of the inclusion size distributions [6, 11–15]. It is observed that the inclusion sizes obtained by different methods have the characteristic of statistical distribution, and statistical analysis methods are utilized to estimate the maximum size of inclusions in large volumes of steel. Statistics of extreme values (SEV) method was introduced by Murakami [6], and the predictions accord well with the experimental results. Shi et al. adopted another statistic of extreme value distribution, the generalized Pareto distribution (GPD) method, to predict the size of maximum inclusion in a volume of clean steel [12–14]. Many other researchers also

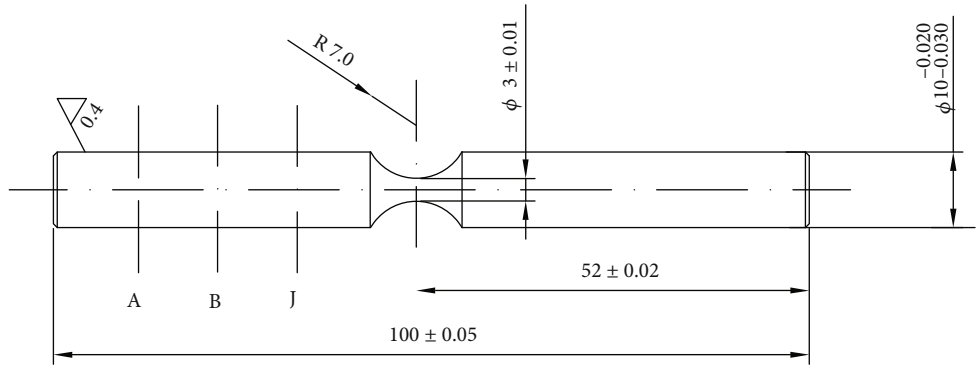

Figure 1: Specimen shape and dimensions for rotating bending fatigue testing.

Table 1: The mechanical properties of the material 40Cr.

Young's modulus (GPa)	Tensile strength (MPa)	Yield strength (MPa)	Elongation (%)	Area reduction (%)	Hardness (HV) (kgf/mm^2)
209	1649	1453	21.13	23.17	523

utilized the two methods to estimate the maximum inclusion size in materials, and their estimation of the maximum inclusion size accords well with the experimental results [16–23]. The methods are also successfully applied for defect statistics of additive manufacturing materials and components [24–28]. Size effect in very high cycle fatigue regime is generally analyzed by considering the statistical distribution of the defects originating the fatigue failures within the risk volume. But there is a case that deserves caution when the optical dark area (ODA) is observed close to the initial defect. It is believed that when the crack starts propagating from the ODA in VHCF, the ODA size in place of the defect size should be considered for the application of the Murakami formulation [29–31].

In this study, both SEV and GPD methods are adopted to predict the maximum inclusion size in 40Cr structural steel, the estimated results were compared with the experimental results obtained in the conventional fatigue test, and the corresponding fatigue strength was estimated according to the obtained maximum inclusion size. All failure-relevant inclusions of the present study were quantitatively analyzed with respect to $\sqrt{\text{area}}$, according to the inclusion rating methodology proposed by Murakami. The advantages and disadvantages of the two methods are discussed, and a critical inclusion size is proposed for material production.

2. Materials and Experimental Procedures

2.1. Experimental Materials. The material adopted in this study is 40Cr structural steel (Chinese standard), which has a chemical composition (wt.%) of 0.39 C, 0.98 Cr, 0.7 Mn, 0.28 Si, 0.2 Ni, and balance Fe. Columnar bars with a diameter of 10 mm were used for specimen manufacturing. Hourglass-shaped specimens were machined with a minimum diameter of 3 mm and a round notch radius of 7 mm, whose dimensions were a little larger than those shown in Figure 1. The raw specimens were austenitized at 860°C for 2 hours and oil quenched and then tempered at 200°C for 1 h and air cooled. Finally, the specimens are machined to precise dimensions with a high precision machine tool. The microstructure of the specimens is tempered martensite, and the mechanical properties are given in Table 1. The average size of the original austenite grains is 10.2 μm measured from 432 grains of intergranular morphology on SEM micrographs taken from fracture surfaces.

2.2. Fatigue Experiments. The rotating bending fatigue experiments were performed in laboratory air by using a cantilever-type rotary bending machine at room temperature, with a stress ratio $R = -1$ and a loading frequency of 50 Hz. Before fatigue testing, the round notch part of the specimen surface was polished by grade 400, 800, 1500, and 2000 abrasive papers. After the specimens were fractured, all fracture surfaces were observed by Scanning Electron Microscopy (SEM), where the crack initiating pattern and inclusion sizes are investigated.

2.3. Inclusion Size Metallographic Examination. To compare the accuracy of the proposed evaluation method with the traditional method, 40Cr steel samples were prepared for surface analysis by optical microscopy. The samples were cut from the ruptured fatigue specimens as shown in Figure 1 (such as A, B, and J) to ensure the consistency of materials. 10 samples with diameter of 10 mm and heights of 10 mm were prepared. The specimen surfaces were mechanically polished and ultrasonically cleaned, and then, an optical microscope (Polyvar Met) was used to inspect the maximum inclusion size on each area. 10-15 visual fields were taken randomly from each sample, with the visual field area $S_0 = 0.04278\,\text{mm}^2$, and 114 visual fields were recorded totally. The inclusions were analyzed by the image analysis software Image Pro Plus v6.0, where the projected areas of inclusions are measured and the parameter $\sqrt{\text{area}}$ (square root of the area) was taken as the characterization of inclusion dimensions.

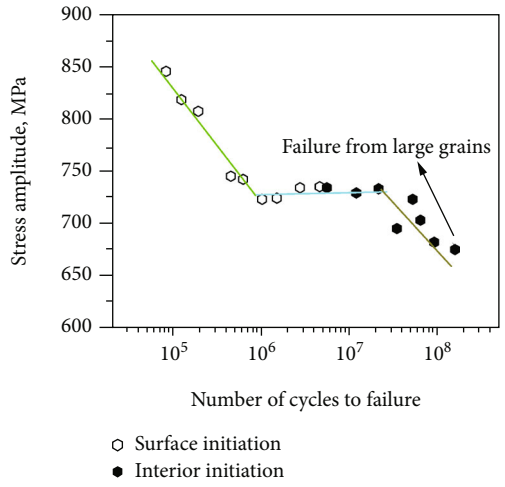

Figure 2: *S-N* curves of 40Cr steel under rotating bending fatigue experiment. Void symbols indicate failure from surface crack initiation, while solid symbols indicate failure from interior crack initiation.

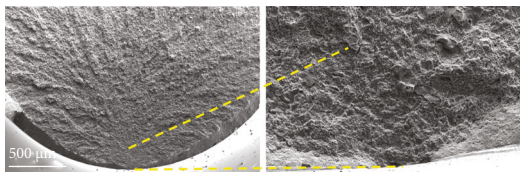

Figure 3: Crack initiation from surface ($\sigma = 744$ MPa, $N = 6.85 \times 10^5$).

3. Experimental Results

3.1. S-N Curve and Fractography of 40Cr Steel. The *S-N* curves of 40Cr steel obtained from rotating bending fatigue experiments are presented in Figure 2. It is seen that the *S-N* curve presents a stepwise descending shape and the specimens continue to rupture until 2×10^8 cycles, which means that the specimens still facture under the conventional fatigue limit. The conventional fatigue limit corresponds to the plateau stress, which is about 715 MPa. Around this stress plateau, the fatigue lifetime could be very dispersed, from 5×10^5 cycles to 5×10^7 cycles.

The typical fracture surfaces of the ruptured specimens were investigated and presented as shown in Figures 3–5. At higher loading amplitude, failure initiated from the specimen surface and resulted in lower fatigue lifetimes (Figure 3). At lower loading amplitude, the fatigue lifetime was relatively higher, and failure initiated from interior inclusions as shown in Figure 4 or interior large grains as shown in Figure 5. In some cases, failure occurred from surface inclusions and resulted in much lower fatigue lifetimes even at a relatively lower loading amplitude.

The dimensions of the inclusions were inspected from the fracture surfaces of ruptured specimens taken by SEM. Due to the irregular shape of the inclusions, the parameter $\sqrt{\text{area}}$ is adopted to characterize the dimensions of the

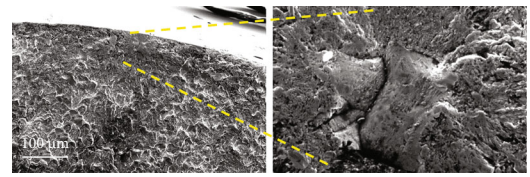

Figure 4: Crack initiation from interior inclusions ($\sigma = 722$ MPa, $N = 5.70 \times 10^7$).

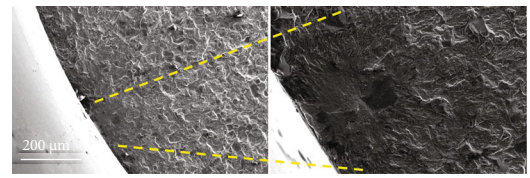

Figure 5: Crack initiation from interior large grains ($\sigma = 674$ MPa, $N = 1.72 \times 10^8$).

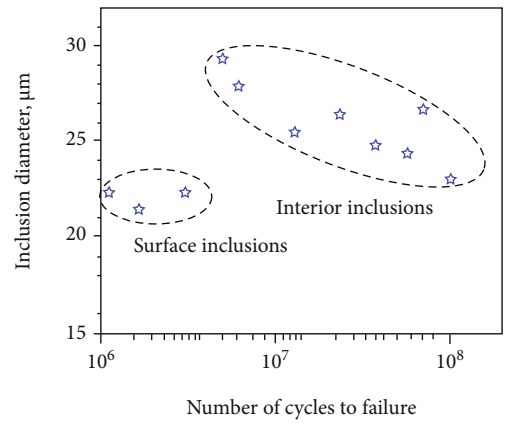

Figure 6: Relationship between inclusion sizes inspected from fracture surfaces and fatigue lifetime.

inclusions. The results are presented in Figure 6. The observed inclusions are in the range of 21.45 μm-29.34 μm. There is a tendency that larger inclusions result in lower fatigue lifetimes, while surface inclusions lead to especially lower fatigue lifetimes.

3.2. Maximum Inclusion Size Estimation by Statistics of Extreme Values (SEV) Method. In the last section, it is seen that the size of inclusion plays an important role in fatigue lifetime; thus, the control of maximum inclusion size is essential in the material manufacturing process. However, it is very difficult to assess the inclusion size in a solid material. Statistics of extreme values (SEV) provides a technical to assess the maximum inclusion size efficiently.

The basic idea of the extreme value theory is that if a fixed number of data points follow a basic distribution (such as normal distribution, logarithmic distribution, and log-normal distribution), then the maximum values of each of these sets also follow a distribution, which is different from

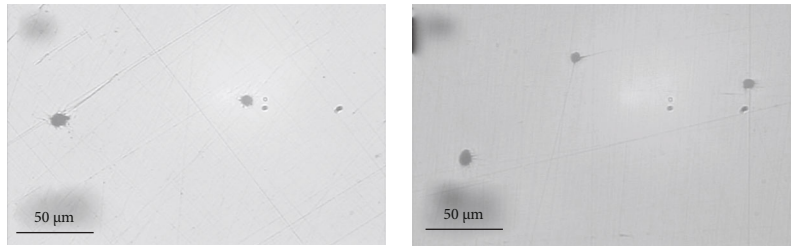

(a) (b)

Figure 7: Optical images captured for inclusion size statics from two samples: (a) sample 2; (b) sample 9.

the basic distribution. The Gumbel distribution is widely used and its distribution function is as follows [6]:

$$G(z) = \exp\left(-\exp\left(-\frac{z-\lambda}{\alpha}\right)\right), \quad (1)$$

where $G(z)$ is the probability that the maximum inclusion is no larger than the size z and λ and α are the location and scale parameters, respectively. Murakami et al. applied this method to the estimation of inclusion size for the first time [6–8]. The estimation process is presented as follows.

(1) N visual fields were observed randomly but not repeated on the sample surfaces, measuring the area of the maximum inclusion in the visual field, defining the size of the inclusion as $X_i = \sqrt{\text{area}}$, and sequencing the number N of X_i: $X_1 \leqq X_2 \leqq \cdots X_i \leqq \cdots \leqq X_{N-1} \leqq X_N$. The cumulative probability of inclusion size not exceeding X_i can be calculated simply by

$$G(X_i) = \exp\left(-\exp\left(-\frac{X_i-\lambda}{\alpha}\right)\right). \quad (2)$$

Indeed,

$$G(X_i) = \frac{i}{N+1}. \quad (3)$$

Based on the two equations above, it is deduced that

$$X_i = \alpha y + \lambda. \quad (4)$$

Here, $y = -\ln(-\ln(i/(N+1)))$. Plot against $X_i - y$, a straight line with slope α and intercept on the vertical axis λ are obtained. In this way, the values of the two parameters could be approximately obtained. The method is named as graphical estimation.

In this study, the typical optical images taken for maximum inclusion size assess are shown in Figure 7. The maximum inclusion sizes are recorded from each image, and totally, 114 values are adopted as shown in Figure 8 ($N = 114$). Through calculation, the estimated results are $\alpha = 1.92$ and $\lambda = 6.15$.

(2) Calculation of return cycle T: the return cycle is also called the total sample size, namely, the ratio of the estimated volume and the observed volume. For the hourglass-shaped samples used in this study, the control volume is calculated as follows [6]:

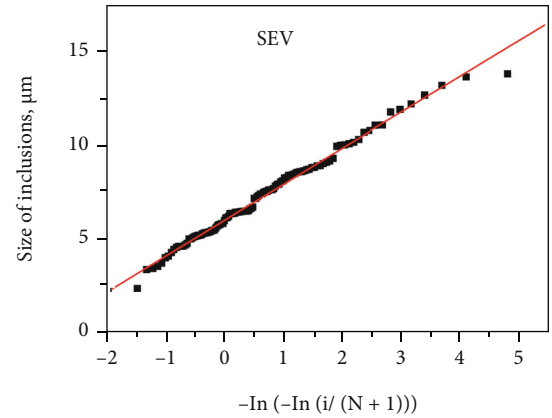

Figure 8: Two parameters of SEV method obtained by plotting.

$$V = 0.25\pi(1-\gamma)(d+d_1)^2 z_1, \quad (5)$$

where $d_1 = d/\sqrt[3]{\gamma}$, $z_1 = \sqrt{R^2 - (R - 0.5(d_1 - d))^2}$, γ is the stress ratio, defined as $\gamma = \sigma/\sigma_0$, σ is the stress at any part of the sample, σ_0 is the maximum stress of the sample, and the control volume is the volume of zone whose stress ratio is larger than γ. R is the radius of the arc part, and d is the diameter of the middle part of sample. In this paper, we have $\gamma = 0.9$, $R = 7$ mm, and $d = 3$ mm. In this study, $V = 2.572\ \text{mm}^3$. Since step (1) is the statistics of area, thus the volume needs to be estimated (the observed area should be converted to volume). An equivalent height is usually defined and set as the average value of the inclusion size.

Equivalent height: $h = \sum_{i=1}^{N} X_i/N = 7.229\ \mu\text{m}$.

Equivalent volume: $V_0 = hS_0 = 3.093 \times 10^{-4}\ \text{mm}^3$.

Return cycle: $T = V/V_0 = 8315$.

The cumulative probability: $G(X_V) = 1 - (1/T) = 0.99988$; accordingly, $y = 9.026$.

The characteristic size of the maximum inclusion in V is preliminarily estimated as

$$X_V = 1.92 \times 9.026 + 6.15 = 23.45\ \mu\text{m}. \quad (6)$$

The maximum likelihood method could also be used to obtain the values of α, λ, and the confidence interval of characteristic size. The likelihood is given by the probability

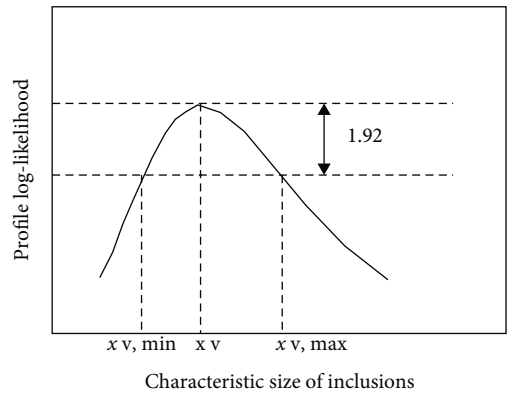

Figure 9: Confidence interval plot.

density functions, and the values of α and λ are obtained when L is the maximum value:

$$L = \prod_{i=1}^{N} \frac{1}{\alpha} \exp\left\{-\left[\frac{X_i - \lambda}{\alpha} + \exp\left(-\frac{X_i - \lambda}{\alpha}\right)\right]\right\}. \quad (7)$$

Through numerical calculation, the values of α and λ when L gets the maximum value are the parameters to be solved.

The confidence interval of the characteristic size of maximum inclusion can be obtained by the profile likelihood function. Different given values of characteristic size X_V will correspond to different maximum likelihood function values L, against which the $\ln L - X_V$ graph is plotted to obtain the profile likelihood function graph, as shown in Figure 9. X_V corresponding to the peak value is the characteristic size of the maximum inclusion estimated in the volume of V. Decrease by 1.92 from the peak value on both sides and correspond to the 95% confidence interval. Define $G^2 = 2\{\ln L(X_V^*) - \ln L(X_V)\}$, and then, G^2 corresponds to the $\chi^2(1)$ distribution. When the confidence level gets 95%, $\alpha = 0.05$ and the value corresponding to $\alpha = 0.05$ is 3.84, so it should decrease from the peak value by 3.84/2 = 1.92. VC++ coding calculation is adopted and the estimated parameters are $\alpha = 1.950$ and $\lambda = 6.135$, and the corresponding characteristic size is $X_V = 23.75\,\mu$m. Compared with the results of plotting, the difference of them is very small and its 95% confidence interval is $[21.23, 26.84]\,\mu$m as shown in Figure 9. The code for maximum characteristic size X_V and confidence interval calculation is provided as a supplementary material.

3.3. Maximum Inclusion Size Estimation by Generalized Pareto Distribution (GPD). The generalized Pareto distribution (GPD) is a family of statistical distributions; the difference between GPD and the statistics of extreme values (SEV) lies in that it arises as exceedances over some threshold. Originally, GPD function was widely applied in the estimation of environmental parameters such as wave peak height, wind velocity, and rainfall. It was firstly adopted by Shi et al. [12–16] to predict the size of maximum inclusion in clean steel, which was subsequently accepted by many other researchers [17, 18].

For a set of data those could be collected, suppose both the number n and their values X_i are random variables. Setting u as the threshold value, X is the size of inclusion larger than u, and then, the inclusions with size larger than u will conform to Poisson distribution. The cumulative probability of inclusion could be expressed with generalized Pareto distribution:

$$F(x) = 1 - \left(1 + \frac{\xi(x-u)}{\sigma'}\right)^{-1/\xi}, \quad (8)$$

where $\sigma' > 0$ is a scale parameter and $\xi(-\infty<\xi<\infty)$ is a shape parameter.

The estimation process is carried out as follows.

(1) Select and sequence inclusions with the size larger than u in each visual field; plot the threshold u and the mean excess of the inclusion size over the threshold u, take out the linear part, and use the intersection point of the straight line and curve line as the critical threshold value. If the data conform to the generalized Pareto distribution, then the slope of the straight line is $\xi/(1-\xi)$, the intercept is $\sigma'/(1-\xi)$, and values of the two parameters could be preliminarily estimated.

In this study, $u = 1.6\,\mu$m is taken, and there are 803 inclusions larger than this threshold. Plot the threshold u and the mean excess of the inclusion size over the threshold u, as shown in Figure 10. Taking the linear part and the critical threshold value as $3.8\,\mu$m, the straight-line equation is $y = 3.381 - 0.198x$.

Through calculation, $\xi = -0.2469$, $\sigma' = 4.216$.

(2) If X_V is the characteristic size of maximum inclusion and $N_V(u)$ denotes the number of exceedances of u in the unit volume, then

$$N_V(u)V(1 - F(X_V)) = 1. \quad (9)$$

Thus,

$$X_V = u - \frac{\sigma'}{\xi}\left\{1 - (N_V(u)V)^{\xi}\right\}. \quad (10)$$

X_V can be obtained from the parameter values calculated above. The maximum inclusion size estimated by GPD method was extrapolated from limited data; thus, the error is inevitable. The maximum likelihood method is used to estimate the 95% of the confidence intervals.

When V is large and $\xi < 0$, $[N_V(u)V]^{\xi} << 1$, it is deduced from Equation (9) that

$$X_V = u - \frac{\sigma'}{\xi}. \quad (11)$$

When V is large enough, the size of the maximum inclusion should tend towards a stable value.

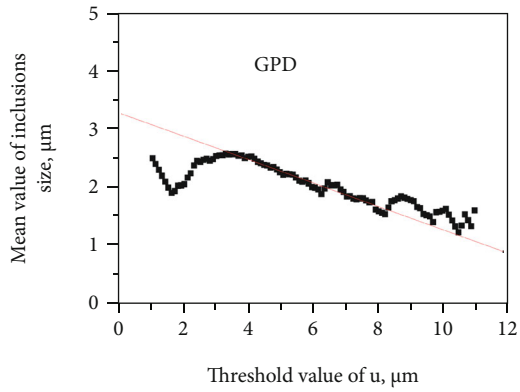

Figure 10: Determination of parameters of GPD method.

In this study,

$$N_V(u) = \frac{\text{number of inclusions larger than } u}{\text{number of inclusions of visual fields} \times V_0} = \frac{239}{114 \times 0.3039 \times 10^{-3}} = 6897. \quad (12)$$

Then, $X_V = 19.35\,\mu$m.

(3) The parameters and confidence interval are further estimated by the maximum likelihood method. The maximum likelihood function is

$$L = \prod_{i=1}^{k} \frac{1}{\sigma'} \left\{1 + \frac{\xi(X_i - u)}{\sigma'}\right\}^{-1/\xi - 1}. \quad (13)$$

Through calculation, $\xi = -0.2437$, $\sigma' = 4.170$, the characteristic size of the maximum inclusion is $X_V = 19.33\,\mu$m, and its confidence interval is $[13.23, 39.33]\,\mu$m.

4. Results and Discussion

4.1. Comparison of Estimation by SEV and GPD Methods with Experimental Results. As indicated by the fatigue testing of 40Cr steel, fractures still occur when the fatigue life is more than 10^7 cycles and the cracks initiate from internal large inclusions. The inclusion sizes obtained by the two statistical methods of extreme values are compared with the experimental results, as shown in Table 2. The estimation results of these two methods are very close to the actual results. The inclusion sizes obtained by the SEV method are a little larger. This is comprehensible that the data used by the SEV method is the maximum value in each visual field, but the GPD method uses the data exceeding a certain threshold. Therefore, the estimation results of the SEV method are comparatively conservative, and the results estimated by the GPD method are closer to the actual results, but the confidence interval is larger.

Table 2: Comparison of inclusion sizes estimated by SEV method and GPD method.

Method	Inclusion size (μm)	Confidence interval (μm)
SEV	23.74	(21.24, 26.84)
GPD	19.33	(13.23, 39.33)
Fatigue test values	29.34, 27.91, 26.65, 25.50, 24.37, 22.31, 21.45	

According to the semiempirical equation proposed by Murakami et al. for predicting the fatigue strength [6],

$$\sigma_w = \frac{C(\text{HV} + 120)}{(\sqrt{\text{area}})^{1/6}}, \quad (14)$$

where HV is the matrix hardness and HV = 523 kgf/mm^2 for 40CrA in this study; C is the parameter related to the inclusion location: $C = 1.41$ for surface inclusions, $C = 1.43$ for subsurface inclusions, and $C = 1.56$ for interior inclusions.

Table 3 presents the comparison of the predicted fatigue strengths and experimental results. It is seen that the predictions of the two methods are close to the experimental results. This indicates that the two methods could predict the very high cycle fatigue performance.

The estimation result of maximum inclusion size in 40Cr steel of different weights is presented in Figure 11, and the error bar is 95% confidence interval. The estimated maximum inclusion size from both the SEV and GPD methods are similar for a small volume of material but diverges for larger volumes. For the SEV method, the estimated maximum inclusion size increases approximately linearly with the increase of the logarithm of the mass of materials, and there is no upper limit for the estimated inclusion size. For the GPD method, the estimated size also increases with the volume of material but there is an upper limit, which is the maximum size of inclusion whatever the volume of steel. The increase of maximum inclusion size with the volume of testing specimen is also validated by the researchers.

4.2. Estimation of Critical Inclusion Size. The previous studies have shown that larger inclusions will greatly decrease the fatigue behavior of materials. According to the Murakami model, the smaller the inclusion in steel, the higher the fatigue strength is, and it is inversely proportional to the power of one-sixth of the size. Thus, it is of great importance to control the inclusion sizes during the material production process. However, the smaller the inclusions are, the higher requirements it needs for the metallurgical technology and the larger the cost is. Besides, the improvement of fatigue behavior is not very obvious when the inclusion size reaches a critical size, below which smaller inclusion size will not lead to higher fatigue strength. Yang et al. [17] conducted an experiment on the industrial 42CrMo steel containing a large number of inclusions (maximum inclusion size 40 μm) and clean 42CrMo steel with inclusion size smaller than 1 μm, and the results indicated that the clean steel had no fatigue fracture at the life interval 10^6–10^9, but many specimens made from industrial steel fractured within

Table 3: Comparison of fatigue limits predicted by the two methods and the experimental results.

Method	Fatigue strength (MPa)			
	σ_{w1} ($C = 1.41$)	Confidence interval ($C = 1.41$)	σ_{w2} ($C = 1.56$)	Confidence interval ($C = 1.56$)
SEV	636	(623, 648)	704	(689, 717)
GPD	659	(585, 701)	728	(647, 776)
Experimental result		720 ± 40		

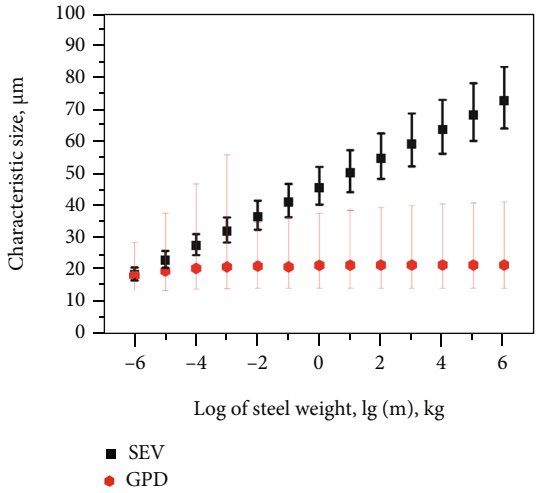

Figure 11: Estimation of maximum inclusions in steel of different weights by the two methods.

this regime. Taking the fatigue strength corresponding to 10^9 as example, the fatigue strength of clean steel is 1.10 times as large as that of industrial steel, instead of the predicted result 1.85 by the Murakami model ($(40\,\mu m/1\,\mu m)^{1/6} = 1.85$). If the grain size of clean steel is used to replace the maximum inclusion size, the predicted result is 1.17 ($(40\,\mu m/15\,\mu m)^{1/6} = 1.17$), which is much closer to the experimental result (1.10). It is also shown in our fatigue experiments that big irregular grains will also act as failure originating site when larger inclusions are absent as shown in Figure 5. To balance the improvement of fatigue behavior and economy of material production process, a critical inclusion size is proposed, below which the inclusions are not dangerous.

For medium and low strength steels, there is a simple linear relationship between fatigue limit and hardness [6]:

$$\sigma_\omega \cong 1.6\mathrm{HV}. \tag{15}$$

By Equation (15) and the semiempirical equation proposed by Murakami, the critical inclusion size may be approximately obtained as

$$\phi \cong 0.8591\left(1 + \frac{120}{\mathrm{HV}}\right)^6. \tag{16}$$

However, Equation (15) only applies to medium and low strength steel. For high strength steel, such as 40Cr steel, its fatigue strength (720 MPa) is much smaller than 1.6 Hv (837 MPa), so the critical inclusion size obtained from Equation (16) is conservative, being 2.92 μm. If 720 MPa is taken as the fatigue limit, the calculated critical inclusion size is 7.31 μm, which is close to the average grain size of the prior austenite (10 μm). Therefore, it is approximately considered that if the maximum inclusion size in production process is controlled below the average grain size, the adverse effects of inclusions may be well alleviated.

5. Conclusions

Two statistic methods, SEV and GPD methods, are applied to estimate the characteristic size of maximum inclusion in 40Cr steel, and then, the fatigue strength is predicted according to the estimated characteristic size of maximum inclusion and compared with the experimental results. The conclusions are reached as follows:

(1) The rotating bending fatigue testing results showed that failure still occurs below the conventional fatigue limit and tends to initiate from interior large no-metallic inclusions. The conventional fatigue limit is about 720 MPa, and the inclusion sizes observed on the facture surfaces are in the range of (21.45, 29.34)

(2) 114 visual fields captured from 10 samples (cut from the ruptured fatigue specimens) are used for inclusion size statics. The estimated maximum inclusion size from both the SEV and GPD methods is similar for a small volume of material but diverges for larger volumes. For the SEV method, the estimated maximum inclusion size increases approximately linearly with the increase of the logarithm of the mass of materials, and there is no upper limit for the estimated inclusion size. For the GPD method, the estimated size also increases with the volume of material but there is an upper limit, which is the maximum size of inclusion whatever the volume of steel

(3) A critical maximum inclusion size about the size of prior austenite grain is proposed for the inclusion size control in material production. It is suggested that if the maximum inclusion size is smaller than the prior austenite grain size, the unfavorable effect of inclusions could be well alleviated

Data Availability

The data presented in this study are available on request from the corresponding author.

Consent

Consent is not applicable.

Conflicts of Interest

The authors declare no conflict of interest.

Authors' Contributions

Zhao Yingxin was responsible for conceptualization, methodology, investigation, formal analysis, writing—original draft, and funding acquisition. Zhao Aiguo was responsible for writing—review and editing.

Acknowledgments

The project is supported by the Research Project of China Academy of Railway Sciences Corporation Limited (2021YJ150).

Supplementary Materials

The code for maximum characteristic size X_V and confidence interval calculation in SEV method is provided as a supplementary material, which could be run by VC++. *(Supplementary Materials)*

References

[1] S. Suresh, *Fatigue of Materials*, Cambridge University Press, Cambridge, 2012.

[2] X. Pan and Y. Hong, "High-cycle and very-high-cycle fatigue behaviour of a titanium alloy with equiaxed microstructure under different mean stresses," *Fatigue and Fracture of Engineering Materials and Structures*, vol. 42, no. 9, pp. 1950–1964, 2019.

[3] A. Zhao, J. Xie, C. Sun, Z. Lei, and Y. Hong, "Effects of strength level and loading frequency on very-high-cycle fatigue behavior for a bearing steel," *International Journal of Fatigue*, vol. 38, pp. 46–56, 2012.

[4] R. Aigner, M. Leitner, M. Stoschka, C. Hannesschläger, T. Wabro, and R. Ehart, "Modification of a defect-based fatigue assessment model for Al-Si-Cu cast alloys," *Materials*, vol. 11, no. 12, article 2546, 2018.

[5] C. Gu, J. Lian, Y. Bao, Q. Xie, and S. Münstermann, "Microstructure-based fatigue modelling with residual stresses: prediction of the fatigue life for various inclusion sizes," *International Journal of Fatigue*, vol. 129, article 105158, 2019.

[6] Y. Murakami, *Metal fatigue: effects of small defects and nonmetallic inclusions*, Academic Press, Cambridge, Massachusetts, United States, 2019.

[7] M. L. Zhu, J. Long, and F. Z. Xuan, "Fatigue life and mechanistic modeling of interior micro-defect induced cracking in high cycle and very high cycle regimes," *Acta Materialia*, vol. 157, pp. 259–275, 2018.

[8] X. Pan and J. Yang, "Probable maximum sizes of inclusions predicted by SEV and PSD for BH steels of automobile exposed panel with different sulfur contents," *Metals*, vol. 10, no. 5, article 637, 2020.

[9] R. Aigner, S. Pomberger, M. Leitner, and M. Stoschka, "On the statistical size effect of cast aluminium," *Materials*, vol. 12, no. 10, article 1578, 2019.

[10] C. Gu, M. Wang, Y. Bao, F. Wang, and J. Lian, "Quantitative analysis of inclusion engineering on the fatigue property improvement of bearing steel," *Metals*, vol. 9, no. 4, article 476, 2019.

[11] Z. Cao, Z. Shi, F. Yu, G. Wu, W. Cao, and Y. Weng, "A new proposed Weibull distribution of inclusion size and its correlation with rolling contact fatigue life of an extra clean bearing steel," *International Journal of Fatigue*, vol. 126, pp. 1–5, 2019.

[12] G. Shi, H. V. Atkinson, C. M. Sellars, C. W. Anderson, and J. R. Yates, "Computer simulation of the estimation of the maximum inclusion size in clean steels by the generalized Pareto distribution method," *Acta Materialia*, vol. 49, no. 10, pp. 1813–1820, 2001.

[13] C. W. Anderson, G. Shi, H. V. Atkinson, and C. M. Sellars, "The precision of methods using the statistics of extremes for the estimation of the maximum size of inclusions in clean steels," *Acta Materialia*, vol. 48, no. 17, pp. 4235–4246, 2000.

[14] C. W. Anderson, J. Mare, and H. Rootzen, "Methods for estimating the sizes of large inclusions in clean steels," *Acta Materialia*, vol. 53, pp. 2295–2304, 2005.

[15] K. V. Anderson and S. R. Daniewicz, "Statistical analysis of the influence of defects on fatigue life using a Gumbel distribution," *International Journal of Fatigue*, vol. 112, pp. 78–83, 2018.

[16] H. V. Atkinso and G. Shi, "Characterization of inclusions in clean steels: a review including the statistics of extremes methods," *Progress in Materials Science*, vol. 48, no. 5, pp. 457–520, 2003.

[17] Z. Yang, S. Li, J. Zhang et al., "The fatigue behaviors of zero-inclusion and commercial 42CrMo steels in the super-long fatigue life regime," *Acta Materialia*, vol. 52, no. 18, pp. 5235–5241, 2004.

[18] D. Zeng, L. Lu, and J. Zhang, "A method to rapidly and accurately evaluate the maximum inclusion size in medium strength steel," *Journal of Materials Research*, vol. 31, no. 18, pp. 2817–2824, 2016.

[19] M. Fitzka, B. Pennings, U. Karr et al., "Influence of cycling frequency and testing volume on the VHCF properties of 18Ni maraging steel," *Engineering Fracture Mechanics*, vol. 216, article 106525, 2019.

[20] J. Lee, S. Y. Park, and B. H. Choi, "Evaluation of fatigue characteristics of aluminum alloys and mechanical components using extreme value statistics and C-specimens," *Metals*, vol. 11, no. 12, article 1915, 2021.

[21] B. J. Schafer, P. Sonnweber-Ribic, H. Ul-Hassan, and A. Hartmaier, "Micro-mechanical modeling of fatigue crack nucleation around non-metallic inclusions in martensitic high-strength steels," *Metals*, vol. 9, no. 12, article 1258, 2019.

[22] X. An, Z. Shi, H. Xu et al., "Quantitative examination of the inclusion and the rotated bending fatigue behavior of SAE52100," *Metals*, vol. 11, no. 10, article 1502, 2021.

[23] M. Oberreiter, S. Pomberger, M. Leitner, and M. Stoschka, "Validation study on the statistical size effect in cast aluminium," *Metals*, vol. 10, no. 6, article 710, 2020.

[24] S. Romano, A. Brandão, J. Gumpinger, M. Gschweitl, and S. Beretta, "Qualification of AM parts: extreme value statistics applied to tomographic measurements," *Materials & Design*, vol. 131, pp. 32–48, 2017.

[25] O. Andreau, E. Pessard, I. Koutiri, P. Peyre, and N. Saintier, "Influence of the position and size of various deterministic defects on the high cycle fatigue resistance of a 316L steel manufactured by laser powder bed fusion," *International Journal of Fatigue*, vol. 143, article 105930, 2021.

[26] V. Sandell, T. Hansson, S. Roychowdhury et al., "Defects in electron beam melted Ti-6Al-4V: fatigue life prediction using experimental data and extreme value statistics," *Materials*, vol. 14, no. 3, article 640, 2021.

[27] N. M. Hamidi, S. Romano, D. Gastaldi, S. Beretta, and M. Vedani, "Combined effect of surface anomalies and volumetric defects on fatigue assessment of AlSi7Mg fabricated via laser powder bed fusion," *Additive Manufacturing*, vol. 34, article 100918, 2020.

[28] Y. N. Hu, S. Wu, Z. Wu et al., "A new approach to correlate the defect population with the fatigue life of selective laser melted Ti-6Al-4V alloy," *International Journal of Fatigue*, vol. 136, article 105584, 2020.

[29] A. Tridello, C. Boursier Niutta, F. Berto, and D. S. Paolino, "Size-effect in very high cycle fatigue: a review," *International Journal of Fatigue*, vol. 153, article 106462, 2021.

[30] S. Invernizzi, F. Montagnoli, and A. Carpinteri, "Experimental evidence of specimen-size effects on EN-AW6082 aluminum alloy in VHCF regime," *Applied Sciences*, vol. 11, no. 9, article 4272, 2021.

[31] Y. Furuya, "Notable size effects on very high cycle fatigue properties of high-strength steel," *Materials Science and Engineering A*, vol. 528, no. 15, pp. 5234–5240, 2011.